Preliminary Test Results of Variable IF Tracking Loop (VITAL) for GNSS Signals

Chun Yang	Thomas Pany	Andrey Soloviev
Sigtem Technology, Inc.	*University FAF Munich*	*QuNav. LLC*
San Mateo, CA 94402	85577 Neubiberg, Germany	Ft. Walton Beach, FL 32548

BIOGRAPHIES

Dr. Chun Yang received his Bachelor of Engineering from the Northeastern University (Shenyang, China) and the title of Docteur en Science from the Université de Paris-Sud (Orsay, France). After postdoctoral research at the University of Connecticut (Storrs, CT), he has been working on adaptive array and baseband signal processing for GNSS, radar, and communications systems and nonlinear state estimation in such applications as target tracking, integrated inertial navigation, and information fusion. Dr. Yang is the winner of 2009 IEEE NAECON Grand Challenge and the recipient of 2007 ION Samuel Burka Award.

Prof. Thomas Pany is with the University FAF Munich/Germany at the faculty of aerospace engineering where he teaches satellite navigation. His research includes GNSS signal processing (in particular for Galileo second generation), GNSS receiver design and GNSS/INS integration. In particular he is developing a modular GNSS test bed for advanced navigation research. Previously he worked for IFEN GmbH and IGASPIN GmbH and is the architect of the SX3 software receiver.

Dr. Andrey Soloviev is a Principle at Qunav. Previously he served as a Research Faculty at the University of Florida and as a Senior Research Engineer at the Ohio University Avionics Engineering Center. He holds B.S. and M.S. degrees in applied mathematics and physics from Moscow Institute of Physics and Technology and a Ph.D. in electrical engineering from Ohio University. His research interests focus on all aspects of GNSS signal processing and estimation, as a well as multi-sensor fusion for navigation applications. He is a recipient of the ION Early Achievement Award and the RTCA William E. Jackson Award.

ABSTRACT

Correlation at an intermediate frequency (IF) produces a composite correlation function made of an envelope being that of the underlying code and an internal structure being that of the IF carrier. The IF carrier correlation introduces zero-crossings to the code correlation as if it pinches the code correlation envelope at the zero-crossing points, having the effect of creating a main peak and several secondary peaks. The quick decay towards zero-crossings sharpens the main peak, which is desired for accurate timing of the direct signal while isolating close-in multipath and spoofing signals. The functionality of variable IF correlation (VIC) in acquisition and its multipath performance are analyzed in a recent paper, together with its lock onto the main peak among secondary peaks without ambiguity and false lock. In this paper, the implementation of VIC into a variable IF tracking loop (VITAL) is presented. A publically available open-source software GPS receiver is modified into VITAL by simply replacing the conventional correlators using a half-chip spacing with the VIC using a spacing of one eighth cycle of IF. The modified software receiver is then used to demonstrate VITAL on real-world GPS C/A-code signals. The preliminary testing results show an increased code tracking accuracy as well as an increased performance positioning results.

INTRODUCTION

The emerging idea of performing correlation at a variable intermediate frequency (IF), known as variable IF correlation (VIC) [Yang, 2015; 2016], offers a means to resolve the conflicting requirement on the shape of correlation function when used in acquisition vs. tracking of a GNSS signal. Due to the discrete nature of search, the acquisition mode desires a correlation function that possesses a large footprint, thus reducing the total number of search grids (search time) needed to cover a large time-frequency uncertainty zone. In contrast, it is preferred to have a sharp correlation function in the tracking mode so as to mitigate the effect of multipath and spoofing signals on the determination of code delay errors. Such a conflicting requirement cannot be satisfied by the conventional correlation implemented in the baseband that has a fixed shape and size.

Indeed, most GNSS receivers perform their acquisition and tracking of code and carrier separately and independently in the baseband with possible rate aiding of carrier to code [Kaplan and Hegarty, 2006; Borre et al., 2007; Pany, 2010]. Such a design

has its practical and cost advantages. However, the baseband signal tracking eliminates the possibility of carrier correlation (the upper limit of measurement resolution) but relies exclusively on code correlation (the lower limit of resolution).

By up-converting the code replica to a suitable IF, the variable IF correlation (VIC) permits joint code and carrier correlation for acquisition and tracking, which produces a composite correlation function made of those of the code and of the IF carrier, respectively. In other words, the composite correlation function has an envelope being that of the PRN code while its internal structure being that of the IF carrier. The inner carrier correlation introduces zero-crossings to the code correlation envelope, having the net effect of shaping and sharpening the central peak.

The sharpness of correlation peak is of paramount importance in measuring a signal's parameters. The sharper the correlation peak, the more accurate the peak location can be determined. Since the location of peak corresponds to the time of arrival (TOA) of the signal, better timing leads to better ranging and ultimately to better position-fixing. In addition, narrow correlation provides high resolution, which is crucial to isolate the direct signal from, or to reduce the impact of, close-in multipath signals, either naturally occurring (reflections) or man-made (spoofing signals).

The VIC technique has the potential to make the correlation peak of a narrowband BPSK code such as a GPS C/A-code as sharp as that of a wideband code such as a GPS P(Y)-code by properly selecting the IF. As such, the technique may enable a wide range of narrowband communications signals, which have been precluded from being considered for precise timing due to lack of bandwidth in the past, as radio signals of opportunity now for ranging and positioning. In the same vein, it can create a correlation function for a BPSK code to look much like a binary offset carrier (BOC) code [Betz, 1999] but without the risk of false lock on to an ambiguous secondary peak. This is because the variable IF can be adjusted progressively (sequentially or in parallel) to shape and sharpen the correlation function from one unambiguous peak (the BPSK) to multiple resolvable peaks as practical as limited by the chosen IF and sampling rate.

The VIC method is applicable not only to pseudorandom number (PRN) codes on binary phase shift keying (BPSK) modulation [Yang, 2015; 2016] but also to orthogonal frequency division multiplexing (OFDM) signals [Yang and Soloviev, 2017]. Examples of OFDM signals include the European Digital Video Broadcast Terrestrial (DVB-T), Chinese Digital Terrestrial Multimedia Broadcast (DTMB), and U.S. Advanced Television System Committee (ATSC) 3.0, wireless cellular phone long-term evolution (LTE) signals, and wireless local area network Wi-Fi 801.11a, g, n, p. Pilot subcarriers of reference symbols of these OFDM signals are originally designed for channel estimation to improve data demodulation in fading environments. They have been used for timing, ranging, and positioning [Thevenon et al., 2011; Serrant et al., 2011; del Peral-Rosado, 2014; Chen et al., 2015; Shamaei et al., 2016; Yang et al., 2017]. However, the peak width of correlation with pilot subcarriers, which are the sum of quadrature phase-shift keyed (QPSK) continuous waves (CW), is determined by the fixed number and distribution of pilot subcarriers across the transmission band. VIC is shown to provide refined TOA estimation [Yang and Soloviev, 2017].

In the context of generalized GNSS signals [Pany and Yang, 2017], the VIC method shifts the signal spectrum up to high frequencies and makes it asymmetric. Other examples of asymmetric spectra include the possible introduction of a third signal component to an existing Galileo open service signal with a frequency offset and the combined coherent tracking of two legacy GNSS signals, e.g., L5 and L2C; E5b and E6-BC known as metasignal [Paonni et al., 2014]. With higher non-zero frequency components, the asymmetric spectrum signals have a wider Gabor bandwidth than the original signals, thus improving code tracking accuracy. The idea is used in bandpass signal design [Nanzer et al., 2016] and to achieve the fundamental bounds [Bidigare et al., 2012].

The above mentioned rate aiding of carrier (PLL or FLL) to code (DLL) is a popular technique at the signal processing level to take advantage of high accurate carrier tracking. Carrier smoothing of code via the Hatch filter is another method widely used at the measurement level to improve pseudorange. VITAL can be viewed as a third method to improve code tracking accuracy with carrier at the code error discriminator level. In this sense, VIC is extended in this paper from acquisition to tracking. For that purpose, the variable IF tracking loop (VITAL) is introduced with a detailed description of major components that differ from conventional tracking loops. In-the-air GPS signal samples, provided in the CD accompanying the textbook [Borre et al., 2007], are used to illustrate the functionalities of VITAL and its ranging and positioning performance improvements.

The rest of the paper is organized as follows. The variable IF correlation (VIC) is first reviewed. The variable IF tracking loop (VITAL) is then presented. Processing results of both simulated and real GPS signals by VITAL in comparison to conventional tracking are next presented. Finally, the paper is concluded together with an outline of future work.

VARIABLE IF CORRELATION (VIC) AND PROPERTIES

Most GNSS receivers perform correlation at baseband by implementing a form of code delay lock loop (DLL) and carrier phase or frequency lock loop (PLL or FLL). Correlation at baseband has many practical and cost advantages. However, such an implementation leaves the shape of correlation function and its peak size solely determined by the inner structure of the code sequence without exploiting carrier correlation. Carrier correlation has the potential to achieve the upper limit in resolution as illustrated in Fig. 1 and explained below.

Consider an ideal BPSK PRN code with a chip width of T_c, e.g., a maximum length sequence used for GPS C/A-code, as shown in Fig. 1(a). Its power spectrum is a *sinc*-function with the first zero-crossings at $\pm 1/T_c$ as shown in Fig. 1(b). The correlation function is a triangle with its base at $\pm T_c$ on either side as shown in Fig. 1(c). Clearly, the correlation function of a code at baseband is solely determined by the code's inner structure itself.

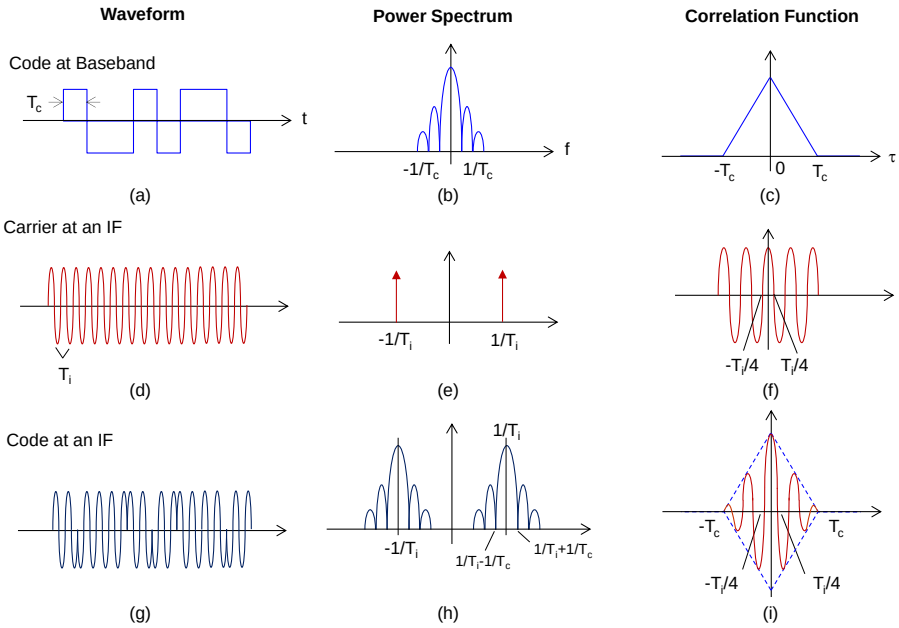

Fig. 1 – Composite Correlation with Code and Carrier

For an IF carrier, the sinusoidal waveform with a period of T_i as shown in Fig. 1(d) has two discrete spectral lines at $\pm 1/T_i$ as shown in Fig. 1(e). Its correlation function is also sinusoidal with the first zero-crossing at $\pm T_i/4$ as shown in Fig. 1(f). Its peaks repeat at a spacing (periodicity) of T_i.

When a baseband code is modulated onto an IF signal with $T_i \leq T_c$ as shown in Fig. 1(g), the resulting spectrum is shown in Fig. 1(h) with $1/T_i \geq 1/T_c$. Although its spectrum is not split about the band center as that of a BOC signal, its correlation function does look like that of a BOC signal as shown in Fig. 1(i). Such a modulation is sometimes referred to as a sinusoidal offset carrier (SOC). The resulting correlation function is made of an envelope being that of the code as in Fig. 1(c) and multiple peaks being those of the IF signal as in Fig. 1(f) but scaled down by the envelope. For easy reference, the shape of waveform or correlation is called a variable IF code/correlation (VIC) and denoted by VIC(f_i, f_c) where $f_c = 1/T_c$ and $f_i = 1/T_i$ (or VIC(f_i/f_0, f_c/f_0) with f_0 = 1.023 MHz being a reference frequency). Clearly, when performing the correlation at an appropriate IF, we can obtain a peak much sharper than that at baseband.

With VIC, the incoming signal is down-converted from f_{RF} to a properly chosen f_i. Obviously, the translation from f_{RF} to f_i can be done in many different ways. At the same time, the local code replica is up-converted from the baseband to f_i prior to correlation at the IF. The correlation at IF in fact involves both the code and the carrier (not the original RF carrier but a translated version at a judiciously chosen IF carrier).

Instead of to a fixed IF, the down-conversion is to a variable IF $f_i \in [0, f_{IF}]$. At an IF, the incoming signal is made of the sample-to-sample products of a code component and a carrier component, and the two can have any phase (timing) relationship and periodicity (frequency) ratio between them (i.e., no coherency between the code and carrier is required, which is a fundamental

difference from BOC). So are the local code and carrier replicas. It is the phase relationship between the incoming signal and the local replica for the code and for the carrier components, respectively, that determines the shape of the correlation function of the composite signal, not the phase relationship between the code and the carrier of the incoming signal or of the local replica.

When the carrier phase error is derived from the normalized in-phase and quadrature components of the prompt correlation, the carrier tracking is "decoupled" from that of code as long as the prompt correlation is above a tracking threshold. As a result, the well-known code-carrier divergence (that is, the code and carrier components move with respect to each other over time in space when the signal propagates through the dispersive ionosphere) does not affect the generation of a code replica and a carrier at IF that can each match up with their counterpart in the incoming signal, being quasi-independent (more on this aspect later on when discussing the VITAL implementation) except for possible rate-aiding from carrier to code with the benefit of narrowing the noise bandwidth of the code tracking loop.

In a GNSS receiver, code tracking and carrier tracking can faithfully follow the incoming signal's variations subject to code delay and phase advance, respectively. However, by themselves and due to the presence of other error terms, the code and carrier phase estimates cannot discern the code-carrier divergence relative to the true timing; side information or another means is needed to mitigate the impact [Sen and Rife, 2008].

The fundamental reason for using a variable IF, rather than a fixed IF, is to ensure smooth and unambiguous transition from fast acquisition to accurate tracking while benefiting from multipath mitigation. As shown in Fig. 1, the one-sided base width Δ of the correlation function at a variable IF $f_i = i/T_c$, denoted by VIC(if_c, f_c) or simply VIC(i, 1) if $f_c = f_0 = 1.023$ MHz, is approximately given by:

$$\Delta = \begin{cases} T_c & i = 0 \\ \sim \dfrac{T_c}{4i} & i > 0 \end{cases} \tag{1}$$

The step size for search in time uncertainty is typically chosen as ½ of the correlation width. Narrower peaks need smaller search steps. Otherwise, a signal appearing between two narrow peaks may be missed without detection. The wider the step, the less the number of search steps is required to cover the same time uncertainty interval. From (1), when the variable IF f_i is doubled, the search step size is reduced in half. As a result, for fast acquisition, a small f_i is recommended.

The higher the variable IF f_i, the narrower the correlation peak is. It provides a better accuracy in determining the peak location and a better resolution in separating close-in multipath signals, thus mitigating the detrimental effects of multipath on timing measurements. As a result, for accuracy and multipath mitigation, a large f_i is recommended.

However, narrowing of the main correlation peak is accompanied by the appearance of secondary peaks of significant strength. Due to noise causing random fluctuations in relative strength of different peaks, a receiver using a delay error discriminator based on early-late correlations runs the risk of false-locking onto a secondary rather than the primary peak, leading to biased timing measurements, which cannot be easily detected and whose correction suffers from a latency. This false lock problem plagues receiver design for the family of BOC codes [Fine and Wilson, 1999].

It is imperative for a BOC receiver to find a way to deal with the difficulty of multi-peak correlation function because the BOC code is fixed so is its multi-peak correlation function. Fortunately, the variable IF tracking architecture circumvents this problem in a natural way. In one implementation, the variable IF tracking mechanism can gradually raise its IF from $f_i = 0$ (i.e., classic code correlation for acquisition) to $f_i = f_{IF}$ (i.e., carrier correlation for fine tracking) while reducing the correlator spacing accordingly. Fig. 2 shows various correlation functions when f_i steps up in a multiple of the chip rate (i/T_c, i = 0, 1, …). Clearly, the main peak width is reduced and secondary peaks appear as f_i steps up. However, different from fixed BOC codes, the variable IF tracking receiver is in complete control of the size and shape of the correlation functions using its variable IF.

When the true signal is not far from to the main peak, the correlation values at three different IF's are rather close as shown in Fig. 2. Since the first zero-crossing of VIC(1, 1) occurs near the secondary peak of VIC(2, 1), a signal that is close to the secondary peak of VIC(2,1) and would be falsely locked on to can be easily detected in conjunction with VIC(1, 1). In Fig. 2, the green squares represent the early-prompt-late correlators placed on VIC(1, 1) and VIC(2, 1), respectively. Although the

prompt channel (the middle green square) is large on VIC(2, 1), it is near zero on VIC(1, 1). The consistency between the prompt channels or lack of is a clear indication of correct lock or false lock.

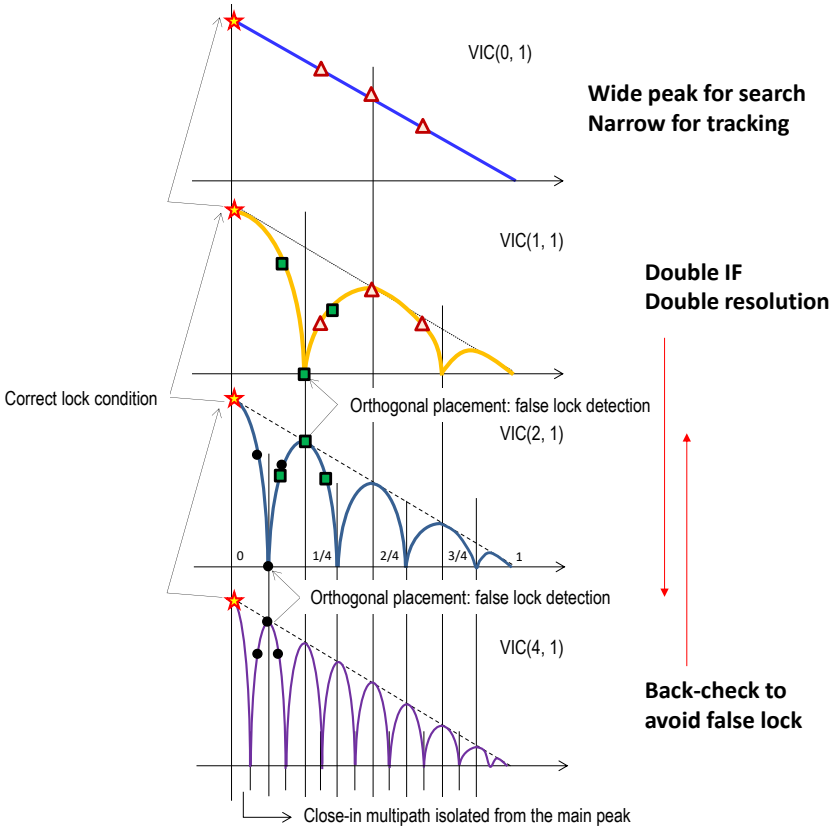

Fig. 2 – Condition for Correct Lock and False Lock Detection

Similarly, the first zero-crossing of VIC(2, 1) occurs near the secondary peak of VIC(4, 1) as shown in Fig. 2. When a signal that is close to the secondary peak of VIC(4, 1) appears, it would be falsely locked on to using the early-prompt-late correlators, which are shown as black dots in VIC(4, 1). Such an ambiguity associated with secondary peaks of significant strength presents a serious challenge to acquisition and tracking of BOC codes because of false lock [Hodgart et al., 2008; Borio, 2014]. Fortunately, the early-prompt-late correlators placed on VIC(2, 1) can easily detect the false lock condition for its prompt value would be below the others rather than reach the maximum as for a correct lock.

Furthermore, any close-in multipath that appears near the main peak can be isolated if it is a resolution away or its influence on the timing estimation is significantly reduced if within the main peak. With the variable IF tracking loop, the main peak width can be adjusted adaptively (the upper limit is set by f_{IF}) to meet multipath mitigation requirements. Beyond a certain limit, there may be no benefit to further reduce the main peak width because the multipath signal is so close that is practically blended into the direct signal.

Simulation results provided in [Yang, 2015; 2016] demonstrated sharpened and unambiguous correlation peaks created by VIC as well as its multipath mitigation. As shown in Fig. 3, the envelopes of delay estimation errors are for the case of a single multipath component with a relative strength of $\alpha_{\text{mp}} = 0.5$. The timing errors in the vertical axis are expressed in terms of samples at $f_s = 10$ MHz for a GPS C/A-code and the relative delay of multipath in the horizontal axis is varied from 0 to 1.5 chips at $f_c = 1.023$ MHz. The conversion factor is about 0.1 chips/sample.

The cyan and green curves are for the C/A code at baseband, a BPSK or equivalently VIC(0, 1), with a wide correlator spacing of $s = ½$ chips and a narrow correlator spacing of $s = 0.1$ chips, respectively. The simulated maximum errors are close to the theoretical values of $\alpha s/2 = 1.25$ samples and 0.25 samples for the wide and narrow correlator spacing, respectively. The top and bottom curves represent the cases when the multipath signal is in phase (0°) and out of phase (180°) with the direct signal.

The red, magenta, blue, and black curves represent the error envelopes for VIC(1, 1), VIC(2, 1), VIC(4, 1) and VIC(8, 1), respectively, which shrink in error magnitude and delay extent progressively. Indeed, the VIC errors are oscillatory with zero-crossings at multiples of a half period and maximum errors at multiples of a quarter period of the corresponding VIC. Timing errors become smaller for multipath signals of larger delays because their sidelobe tails have less effect on the direct signal.

As shown in Fig. 2, VIC(1, 1) is upper-bounced by VIC(0, 1) (i.e., the baseband BPSK code) with a wide correlator spacing while the other VIC's are upper-bounded by VIC(0, 1) with a narrow correlator spacing. The advantage of VIC for multipath mitigation is easily understood because the mainlobe of VIC of a higher order gets sharper. Conventional narrow correlator [van Direndonck et al., 1992] is limited in how small the spacing between E, P, and L can ultimately be reduced due to noise sensitivity, that is, when the spacing is reduced below a certain small value, E, P, and L become practically equal (coalescence) where noise starts to dominate. In contrast, three samples can always be placed on the VIC mainlobe, which is a distinct peak, no matter how sharp it is while still maintaining 3 dB differences between P and E and L, respectively, which is the resolution power of the VIC method.

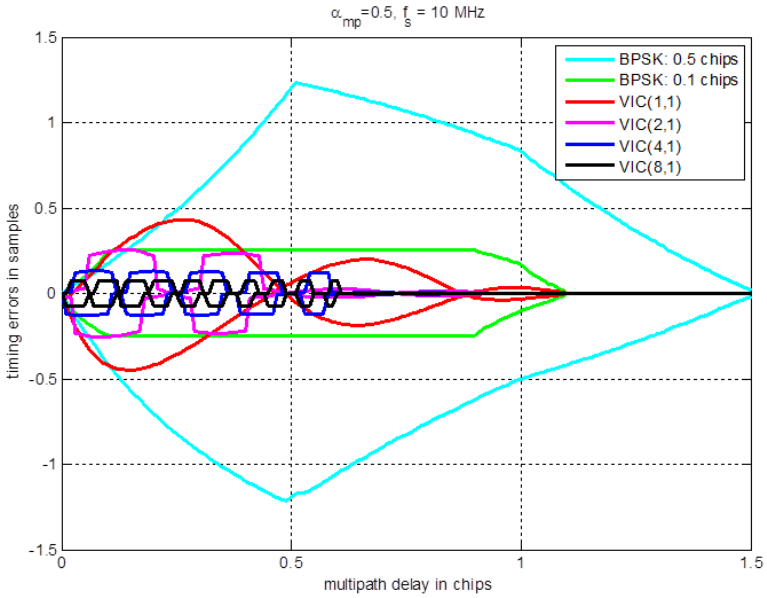

Fig. 3 – Multipath-Induced Delay Estimation Error Envelopes

VARIABLE IF TRACKING LOOP (VITAL) AND IMPLEMENTATION

Fig. 4 shows the essential components of a typical classic baseband tracking receiver. It consists of four subsystems: an antenna, a RF front-end, a baseband signal processor, and a navigation data processor. The in-the-air GNSS signal is captured by the antenna with frequency at $f_{RF} + f_d$ where f_{RF} is the nominal carrier frequency and f_d is a frequency deviation due to line-of-sight (LOS) motion and clock drift.

In its simplest form, the RF front-end down-converts the RF signal at $f_{RF} + f_d$ to an IF signal at $f_{IF} + f_d$ through mixing it with a local signal at f_{LO} derived from a local oscillator (LO) by a frequency synthesizer. The frequency synthesizer also provides a sampling clock f_s to perform analog to digital conversion (ADC) as well as a clock signal to drive the baseband signal processor.

The baseband signal processor further down-converts the sampled IF signal to the baseband by mixing it with a locally generated carrier replica at $f_{IF} + \hat{f}_d$. Then the sampled baseband signal is correlated with several copies of the code, each delayed relative to the other, thus producing the so-called early (E), prompt (P), and late (L) correlations. The in-phase and quadrature-phase components of the prompt correlation (P) are used by the carrier phase error discriminator to derive an estimate of carrier phase errors. The carrier phase error is averaged and scaled in the loop filter to produce an estimate of the carrier frequency deviation $\hat{f}_d$, which, together with the nominal IF frequency f_{IF}, serves as the rate input to the carrier's numerical controlled oscillator (NCO). The carrier NCO generates carrier phase for a waveform generator, which produces a waveform at $f_{IF} + \hat{f}_d$, thus closing the carrier loop.

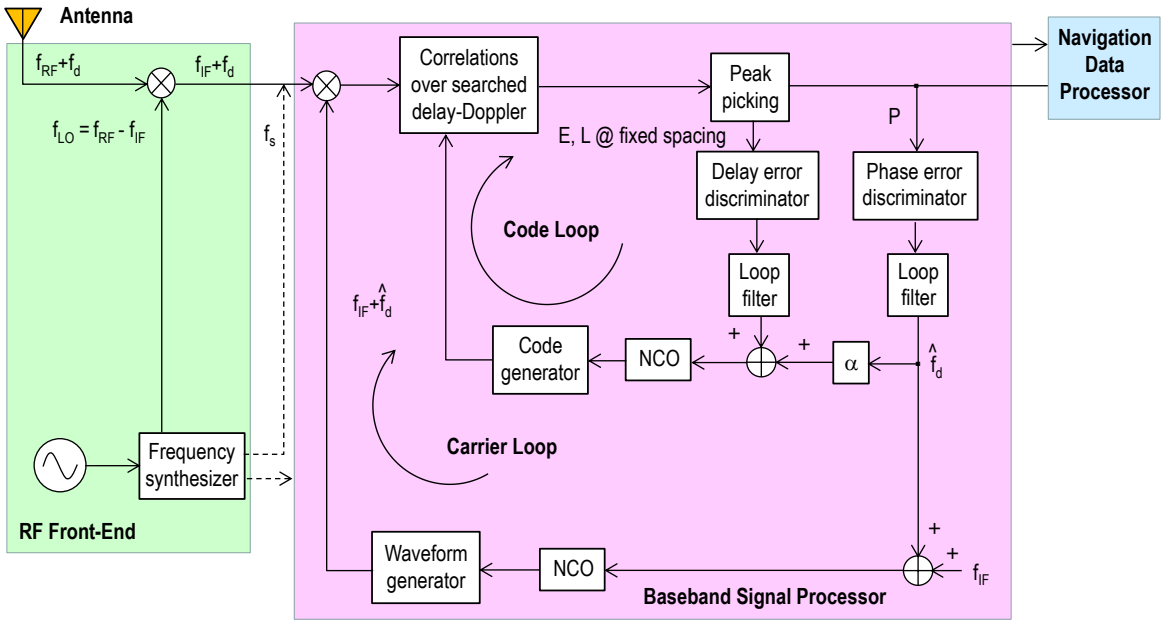

Fig. 4 – Classic Baseband Tracking Architecture

Similarly, the early and late correlations (E and L) are used by the code delay error discriminator to derive an estimate of the code phase error. The code phase error is averaged and scaled in the loop filter to produce an estimate of code frequency error. As shown in Fig. 4, the carrier loop provides a α-scaled version of $\hat{f}_d$ to the code loop for rate aiding. The rate input is used to drive the code's NCO to produce code phase, which in turn is used by the code generator to produce a code replica, thus closing the code loop.

The pair of code and carrier tracking loops as described above is constructed by the baseband signal processor for each visible satellite. The navigation data processor receives code phase, carrier phase and frequency, and data bits from tracking loops for all visible satellites to form pseudoranges, demodulate navigation message, and ultimately to obtain a position fix.

Fig. 5 shows the block diagram of an exemplary implementation of VITAL. Compared to the classic receiver architecture in Fig. 4, there are five major changes for VITAL in Fig. 5:

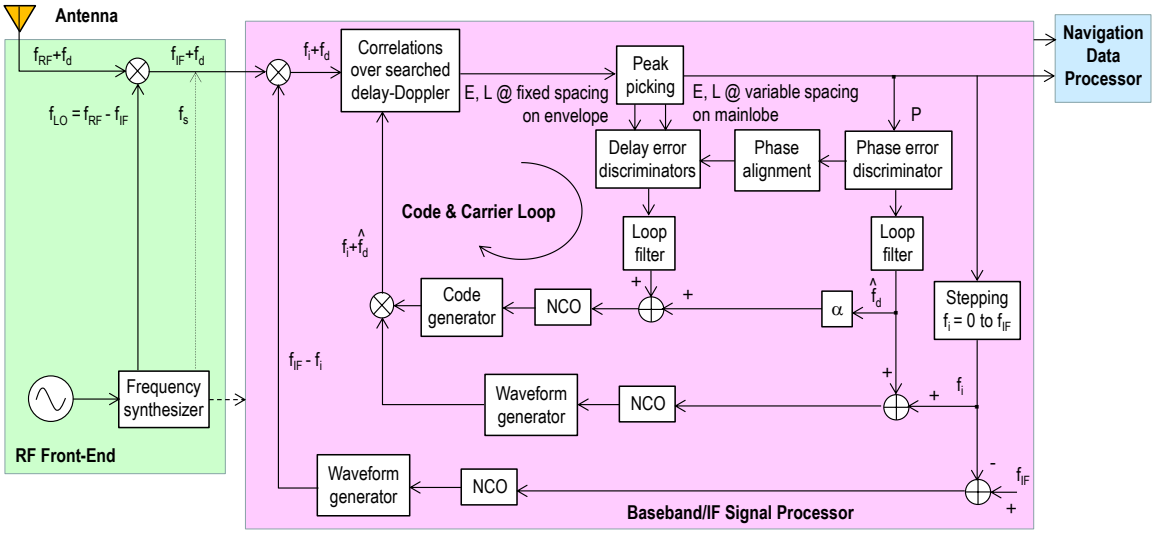

Fig. 5 – Example Implementation Scheme of VITAL

- First, an extra down-conversion stage (a digital mixer) is added for down-conversion to a variable IF at $f_i \in [0, f_{IF}]$. The reference signal at $f_{IF} - f_i$ is produced by a waveform generator (e.g., a sin/cosine look-up table) and a NCO.

- Second, a new decision mechanism is needed to step through the desired values for f_i during the acquisition and tracking process.

- Third, although the structure of code loop remains intact, the carrier loop is modified to up-convert the code replica to the variable IF at f_i plus the estimated frequency error $\hat{f}_d$.

- Fourth, in addition to the carrier frequency to code rate aiding via α, a phase alignment is applied to early, prompt, and late correlations from the carrier phase error discriminator such that the prompt correlation has its peak in the in-phase component and a zero-crossing in the quadrature component. More discussion of this operation is due later in this section

- Fifth, a coarse delay error discriminator transitions to a successively more refined delay error discriminator.

The conventional correlation at baseband is equivalent to VIC(0, 1) as shown in the top plot of Fig. 2 where the normalized early minus late power delay error discriminator with a fixed spacing (typically a ½ chips) can be applied to provide a coarse delay error estimate. When the same delay error discriminator is applied to the mainlobe of VIC(i, 1), with the spacing reduced with an increasing i (typically a ½ width of the half lobe) as shown in the bottom plots of Fig. 2, provides a refined delay error estimate. Such a placement of correlators is further illustrated in Fig. 6 where the absolute value (envelope) of the complex correlation, *abs*(VIC(i, 1)) = *abs*(VIC(0, 1)), is the dashed red-colored curve, and its real part (in-phase component), *real*(VIC(i, 1)), is the solid blue-colored curve.

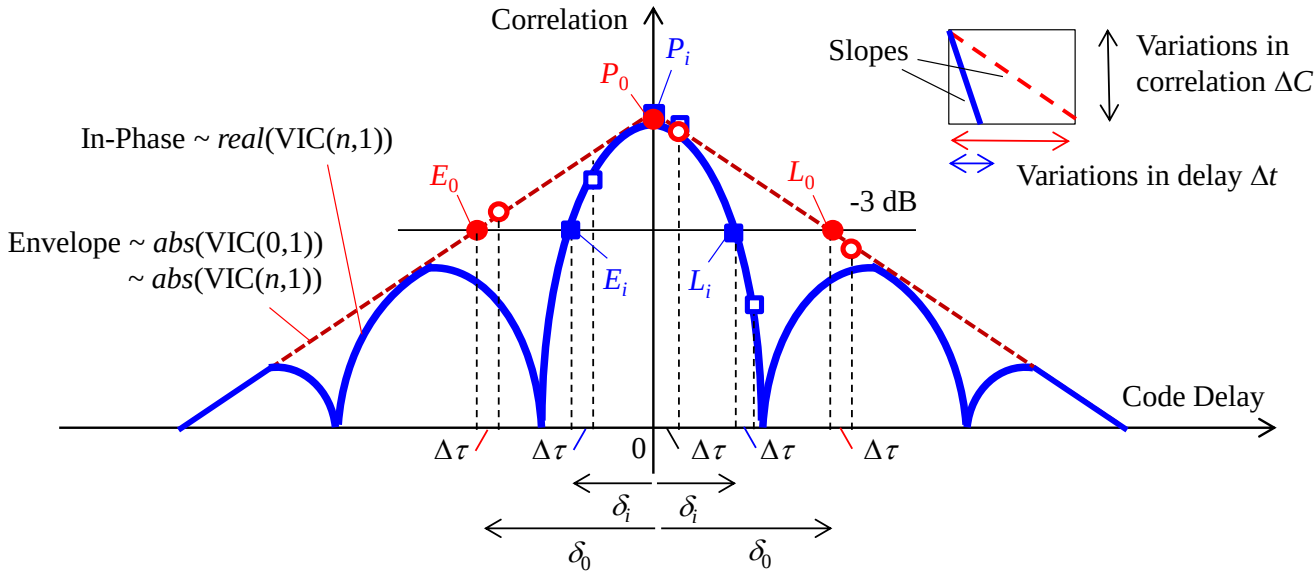

Fig. 6 – Correlations with Fixed Spacing on Envelope and Variable Spacing on Mainlobe

In Fig. 6, for a perfectly aligned incoming signal, the red dots represent the early, prompt, and late correlations with a -3 dB spacing of d_0 on the envelope of *abs*(VIC(n, 1)) = *abs*(VIC(0, 1)), denoted by E_0, P_0, and L_0, respectively. Similarly, the blue solid squares represent the early, prompt, and late correlations with a -3 dB spacing of δ_i on the mainlobe of *real*(VIC(i, 1)), denoted by E_i, P_i, and L_i, respectively. When the incoming signal is mis-aligned by a code delay $\Delta\tau$, the early, prompt, and late correlations are marked as red circles on the envelope and blue squares on the mainlobe of the real component.

A sharper peak can better isolate multipath and spoofing signals. Furthermore, the measurements on the mainlobe with a sharper peak are more sensitive to the incoming delay error and less affected by noise than those on the envelope, which is a kind of data compression effect as showed in the upper right of Fig. 6. The same variation in correlation ΔC (due to noise for instance) produces a smaller delay Δt for a steeper slope from a sharper peak (less noise sensitive). Conversely, the same delay Δt produces a larger change in correlation ΔC again for a steeper slope from a sharper peak (more sensitivity to delay).

As shown in Fig. 5, a simple implementation may adopt a five correlator configuration where P_i coincides with P_0, E_0 and L_0 have a fixed spacing of d_0 whereas E_i and L_i have a variable spacing of δ_i. The use of variable spacing correlators on the mainlobe is a major difference between VIC and BOC. The latter may also have five correlators such as very early (VE), early (E), prompt (P), late (L), and very late (VL) [Fine and Wilson, 1999]. In [O'Driscoll et al., 2016], also used are five correlators: a prompt correlator for phase tracking, an early-late pair of correlators for subcarrier tracking, and the other early-late pair for code tracking. But they are all of fixed spacing and are used primarily for false lock, not for improving accuracy as in VIC.

The incoming signal is modeled, without the noise term, as:

$$x(t) = ab(t-\tau_0)c(t-\tau_0)cos(2\pi(f_{IF}+f_d)t+\varphi_0) \tag{2}$$

where a is the signal amplitude related to the carrier power, $b(\cdot)$ is the data bit, $c(\cdot)$ is the spreading code, τ_0 is the code delay, f_{IF} is the an intermediate frequency at which the signal is sampled, f_d is the Doppler frequency shift (the corresponding code Doppler is omitted from the equation), and φ_0 is the initial carrier phase. For simplicity, other satellite signals are omitted from (2).

In Fig. 5, two local carrier replicas are generated as:

$$dn_i(t) = exp\{j(2\pi(f_{IF}-f_i)t+\varphi_i)\} \tag{3a}$$

$$up_i(t) = exp\{j(2\pi(f_i+\hat{f}_d)t+\phi_0)\} \tag{3b}$$

where $f_i \in [0, f_{IF}]$ is the variable IF and ϕ_i and ϕ_0 are the initial phases for the two local carrier replicas, respectively, which are kept in such a way to ensure the waveform continuity, and $\hat{f}_d$ is the Doppler estimate.

The incoming signal is then down-converted by $dn_i(t)$ to the variable IF f_i as:

$$y(t) = x(t)dn_i^*(t) = ac(t-\tau_0)exp\{j(2\pi(f_i+f_d)t+\theta_i)\} \tag{4a}$$

where the superscript * stands for complex conjugate, the high frequency component is ignored, and $\theta_i = \varphi_0 - \varphi_i$.

Similarly, the code replica is up-converted by $up_i(t)$ to the same variable IF f_i as:

$$z(t) = c(t-\hat{\tau}_0)exp\{j(2\pi(f_i+\hat{f}_d)t+\phi_0)\} \tag{4b}$$

where $\hat{\tau}_0$ is the delay estimate.

Note that (3b) and (4b) represent the carrier and code replicas for the prompt correlation channel. Its output at a variable IF, denoted by $vic(\cdot)$, can be modeled, again without the noise term, as:

$$vic(\Delta\tau, \Delta f) = \int_0^T y(t)z^*(t)dt \tag{5a}$$

$$= aR(\Delta\tau)sinc(\pi\Delta fT)exp\{j(\pi\Delta fT+\Delta\phi_i)\} \tag{5b}$$

$$= aR(\Delta\tau)sinc(\pi\Delta fT)exp\{j(\pi\Delta fT+2\pi(f_i+\Delta f)\Delta\tau_i)\} \tag{5c}$$

where $\Delta\tau = \tau_0 - \hat{\tau}_0$ is the code delay error, $\Delta f = f_d - \hat{f}_d$ is the frequency error, T is the despreading (coherent) integration interval, $\Delta\phi_i$ is the initial carrier phase error, which can be equivalently expressed in terms of IF carrier delay $\Delta\tau_i$ (which is the IF carrier delay and may not necessarily correspond to the code delay $\Delta\tau$) as:

$$\Delta\phi_i = \theta_i - \phi_0 = 2\pi(f_i+\Delta f)\Delta\tau_i \tag{5d}$$

and the code correlation function for an ideal random code is given by:

$$R(\tau) = T\begin{cases} 1 - \dfrac{|\tau|}{T_c}, & |\tau| \le T_c \\ 0, & \text{otherwise} \end{cases} \tag{5e}$$

with the chip duration of T_c, and the *sinc*-function is defined as:

$$\text{sinc}(\pi \Delta f T) = \frac{\sin(\pi \Delta f T)}{\pi \Delta f T} \tag{5f}$$

From (5e), it is easy to verify that the 3 dB-loss of correlation due to timing error is $\tau = T_c/2$ while from (5f), the 3 dB-loss due to frequency error is $\Delta f = 0.6/T$. It explains why the correlator spacing is typically chosen as a half-chip in time and $1/(2T)$ in frequency, respectively, during acquisition.

Consider the prompt correlation in (5). Comparing it to the conventional baseband correlation reveals a major difference, that is, the argument of the complex exponential in (5c) contains an extra term of $2\pi(f_i + \Delta f)\Delta\tau_i$. In fact, this extra term is not a no-show in the conventional baseband correlation but is usually omitted as a second-order effect. Indeed, without f_i, the term becomes proportional to $\Delta f \Delta\tau_i$, which vanishes rather quickly as the tracking loops start converging with $\Delta f \to 0$ and $\Delta\tau_i \to 0$. In the presence of f_i, this term modifies the size and shape of the correlation peak in two ways. Ideally without carrier phase and frequency errors, the mainlobe is dominated by the real part (the in-phase component) as $\cos(2\pi f_i \Delta\tau_i)$, which is the correlation of the IF carrier at f_i. As an example, Fig. 7(a) shows the real component (the blue cross), which reaches its peak at $\Delta\tau_i = 0$ where the imaginary component (the green circle) makes its zero-crossing. However, in the presence of carrier phase and/or frequency errors, the zero-crossing of the imaginary component is shifted so is the location of the peak value of the real component as shown in Fig. 7(b). The envelope (the red plus) remains the same as VIC(0, 1) regardless of any frequency and phase errors. To remove this mismatch, a phase alignment step is taken as follows.

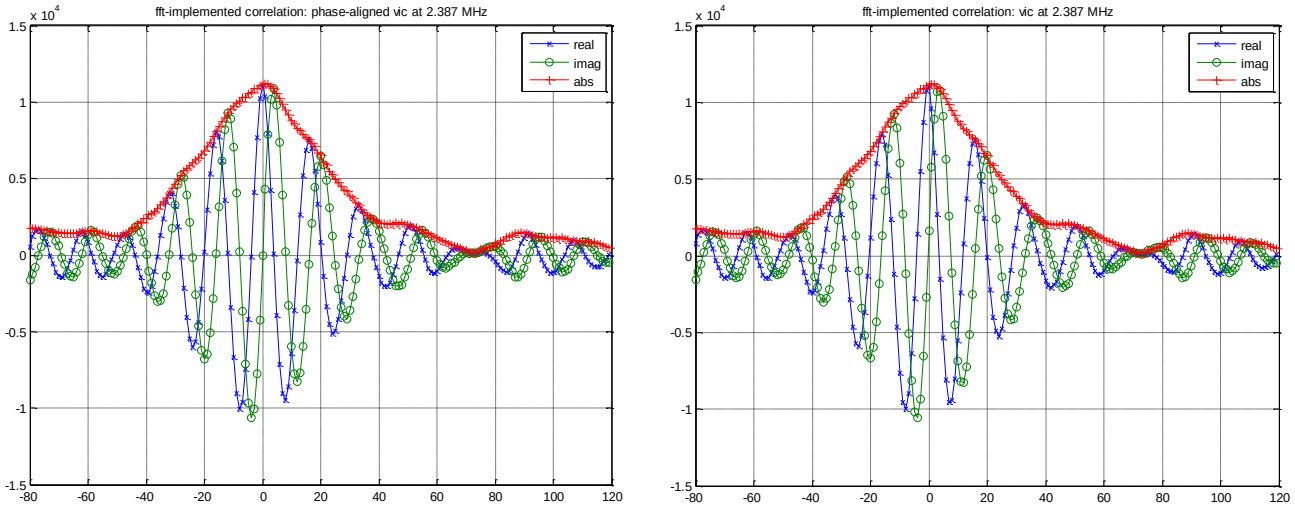

(a) Components of Phase-Aligned VIC(2, 1) (b) Components of VIC(2, 1) with Phase Errors

Fig. 7 – Effect of Phase Errors on Various Components of VIC

First, the envelope tracking is applied right after acquisition, which is then followed by transitioning to the mainlobe tracking at different IF sequentially. To perform the mainlobe tracking at an IF, the aggregated carrier phase error is estimated from the prompt correlation as:

$$\Delta\hat{\theta} = \text{atan}\left(\frac{imag(vic_0(\Delta\tau,\Delta f))}{real(vic_0(\Delta\tau,\Delta f))}\right) \approx \pi\Delta\hat{f}T + \Delta\hat{\phi}_i = \pi\Delta\hat{f}T + 2\pi\left(f_i + \Delta\hat{f}\right)\Delta\hat{\tau}_i \tag{6}$$

where *real*(·) and *imag*(·) stand for the real (in-phase) and imaginary (quadrature) parts of a complex variable. In (6), it is implied that the incremental phase due to frequency errors over T is smaller than the range of arctangent of $\pm\pi/2$ once within

the pull-in range. The carrier phase error $\Delta\hat{\theta}$ is used, on the one hand, to drive the loop filter of PLL and, on the other hand, to phase-align the early and late correlations prior to their use for code phase error estimation.

Indeed, in the tracking mode, after the PLL locks, $\Delta\hat{\theta} \approx 0$. The local IF carrier replica $z(t)$ in (4b) well matches the incoming signal at IF $y(t)$ in (4a) with $\Delta\hat{f} = f_d - \hat{f}_d \approx 0$ and $\Delta\hat{\phi}_i = \theta_i - \phi_0 \approx 0$. Prior to the PLL convergence, multiplying the IF carrier replica with $exp\{j\Delta\hat{\theta}\}$, though noisy, can temporarily phase-align it with the incoming signal at IF.

Regardless of the actual value of $\Delta\hat{\theta}$, we can perform a correlation at IF between the incoming signal and the replica. Both the code and IF carrier replicas are delayed or advanced by $k\delta_i$ relative to the prompt channel timing where $k = 0, \pm 1$ and δ_i is the correlator spacing. Although the code correlation may not change much by $k\delta_i$, the IF carrier correlation introduces a power factor of $cos^2(2\pi k\delta_i) = ½$ (-3 dB) for $f_i\delta_i = 1/8$, as illustrated in both Figs. 6 and 7.

Assume at this point the incoming signal develops a timing disturbance ε to both its code and carrier. As long as it is within the mainlobe, it is felt by the phase-aligned early, prompt, and late correlations without ambiguity as:

$$\tilde{vic}_k(\varepsilon, 0) = vic_k(\varepsilon, 0)e^{-j\Delta\hat{\theta}} \approx aR(\varepsilon + k\delta_i)\exp\{j(2\pi f_i(\varepsilon + k\delta_i))\} \tag{7}$$

The real-parts of phase-aligned early and late correlations can be used to construct a code delay error discriminator as:

$$\frac{real(E_i)-real(L_i)}{real(P_i)} = \frac{real(\tilde{vic}_{-1}(\varepsilon-\delta_i,0))-real(\tilde{vic}_1(\varepsilon+\delta_i,0))}{real(\tilde{vic}_0(\varepsilon,0))} = \frac{\cos(2\pi f_i(\varepsilon-\delta_i))-\cos(2\pi f_i(\varepsilon+\delta_i))}{\cos(2\pi f_i\varepsilon)} \tag{8a}$$

$$= \sqrt{2}tan(2\pi f_i\varepsilon), \quad f_i\delta_i = 1/8 \tag{8b}$$

Alternatively, a polynomial fit (e.g., quadratic) can be applied to the real part of E_i, P_i, and L_i to obtain an estimate of the timing error ε, which is used to drive the loop filter of DLL as implemented in the next section. Note that there are two couplings from the carrier loop to the code loop: one is the rate-aiding via α as shown in Figs. 4 and 5 for both the conventional and VITAL systems; and the other is the phase-alignment in (7) unique to VITAL. Such couplings make code phase estimates correlated to carrier phase estimates as analyzed in [Pany and Yang, 2017]. It is interesting to further study this aspect in a manner similar to combined code and subcarrier phase measurements [Hodgart et al., 2008] and subcarrier-smoothed code phase measurements [Palestini, 2010].

Finally it is interesting to compare VITAL with double estimator (DE) [Hodgart et al., 2008] and double phase estimator (DPE) [Borio, 2014] for BOC signals. The fact that BOC is the product of a spreading code and a periodic subcarrier is recognized in DE by tracking their delays separately with a delay lock loop (DLL) for the code and a subcarrier lock loop (SLL) for the subcarrier. In DPE, the square wave of subcarrier is approximated by a sine wave, which is then tracked by a subcarrier phase lock loop (SPLL). In VITAL, the carrier at a variable IF plays a role similar to that of the BOC subcarrier but it is not a square wave as in DE and rather a sine wave as in DPE. Obviously, a key difference is the ability of controlled change of IF in VITAL.

In a BOC signal, the subcarrier is synchronized to the spreading code at least at transmission so that the well-defined time relationship allows for a joint tracking, a double estimator, or a double phase estimator mentioned above. In VIC, there is no strict time relationship between the spreading code and an arbitrarily chosen IF carrier. For the purpose of correlation peak-sharpening, there is no need to maintain a time relationship between the IF carrier and the code as long as the IF carrier introduces the same amount of transitions (sign flips) to an otherwise "constant" code chip. To use the IF carrier to improve timing, however, it is necessary to align the zero-crossing (or the peak) of the IF waveform with the rising edge of a code chip, leading to a sine VIC – sVIC (or a cosine VIC – cVIC). It is done in VITAL by phase rotation of the prompt correlation into real-valued as in (7). The same phase rotation is applied to the early and late correlations. This is akin to forcing a cVIC with instantaneous alignment of code and subcarrier, which suffices for use in amplitude comparison for refined delay estimation. Such a phase alignment makes finer range measurement possible for it lines up the IF carrier cycles within each code chip as a ruler shorter than the code chip. On the other hand, it also couples any errors in IF carrier phase measurements into those of code phase measurements, a carrier and code correlation previously analyzed in terms of the cross term in the Fisher information matrix in [Pany and Yang, 2017].

TEST RESULTS WITH EXPERIMENTAL DATA

To test the functionality and performance of VITAL, we implemented the scheme shown in Fig. 5 by modifying SoftGNSS V3.0 and ran real GPS data, both provided in the CD accompanying the book [Borre et al. 2007]. For SoftGNSS V3.0, the recorded signal has an intermediate frequency of f_{IF} = 9.548 MHz, sampled at f_s = 38.192 MHz with sample width of 8 bits. A major modification made to SoftGNSS V3.0 is the replacement of the conventional early, prompt, and late correlators spaced by a half-chip with VIC in calculating the code and carrier phase error discriminators used by the DLL and PLL loop filters (2^{nd}-order loops). Another modification is that the time of arrival (TOA) for pseudorange calculation is now retrieved from DLL NCO instead of an integer number of samples (at f_s = 38.192 MHz) in SoftGNSS V3.0.

In the VITAL implementation, the variable IF is chosen to vary on different time slices, that is, from f_i = 0 (0 to 10000 ms), 1.1935 (10001 to 20000 ms), 2.387 (20001 to 30000 ms), and 4.774 MHz (30001 to 37000 ms), corresponding roughly to VIC(0, 1), VIC(1, 1), VIC(2, 1), and VIC(4, 1), respectively. To visualize the whole correlation function at IF, the correlation is calculated using FFT between the incoming signal samples down-converted to f_i and the prompt channel samples up-converted to f_i.

The code phase errors for VIC(0, 1), VIC(1, 1), VIC(2, 1), and VIC(4, 1) are shown in Fig. 8(a), each lasting about 10 seconds, where the code phase errors are calculated from the real components of the correlations spaced by a 1/8 cycle. The conventional normalized early minus late correlation power (NEMLP) with ½ chip spacing is similar to VIC(0, 1) as shown in Fig. 8(b). Since the carrier phase errors are calculated on the in-phase and quadrature components of the prompt correlator, both the VITAL and conventional tracking loop produce similar phase errors as shown in Figs. 8(c) and (d).

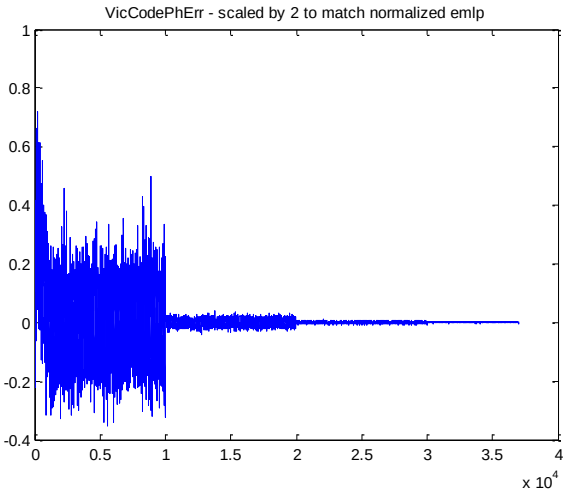

(a) Quadratic fit to early-prompt-late of VIC, spaced by 1/8 cycle, scaled to match conventional NEMLP

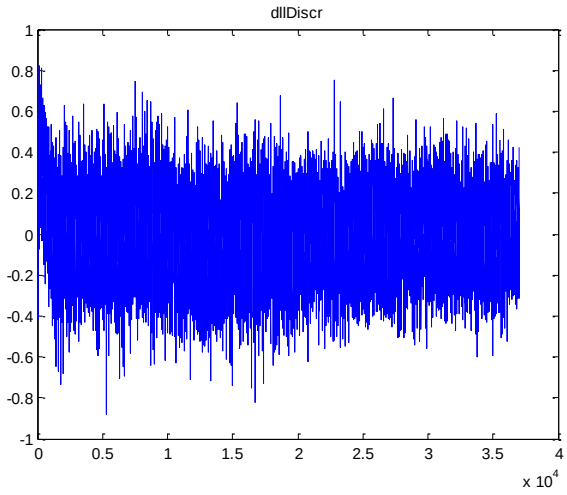

(b) Conventional normalized early minus late correlation power (NEMLP), spaced by ½ chips

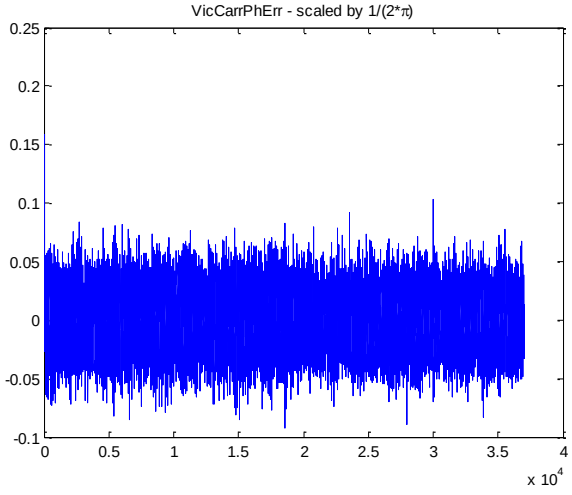

(c) *atan*(·) on the prompt correlator of VIC, scaled

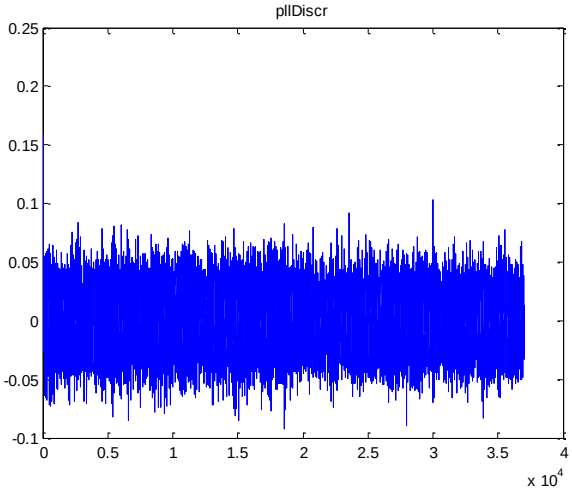

(d) *atan*(·) on the conventional prompt correlator

Fig. 8 – Outputs of Code Phase and Carrier Phase Error Discriminators

Fig. 9 shows the correlations for different IF frequencies over samples away from the prompt code phasing (the zero index). The absolute real (in-phase, blue cross), absolute imaginary (quadrature, green circle), and magnitude (red plus) correlations are plotted. When the carrier phase is aligned, the in-phase component of the prompt has the peak value while the quadrature component has a zero-crossing. For VIC(1, 1), the spacing is 4 samples as shown in Fig. 9(b). For VIC(2, 1), the spacing is 2 samples as shown in Fig. 9(c) with details in Fig. 9(d). For VIC(4,1), the spacing is 1 sample as shown in Fig. 9(e) with details in Fig. 9(f).

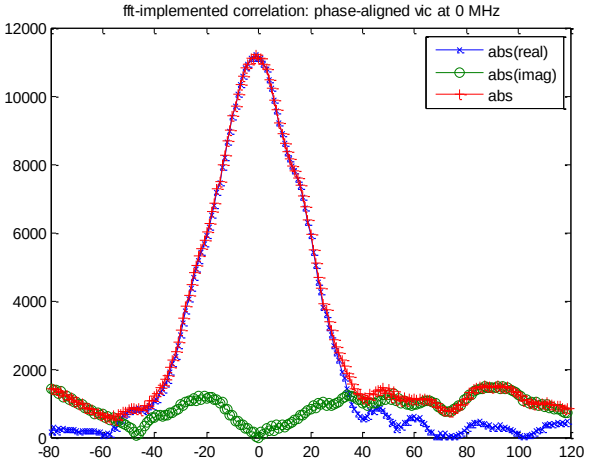

(a) VIC(0, 1) ~ Conventional

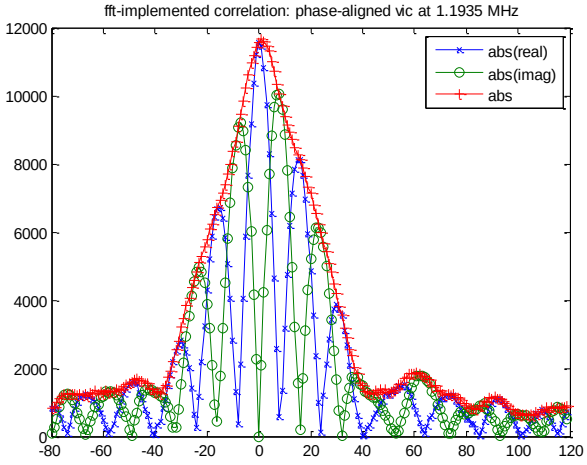

(b) VIC(1, 1)

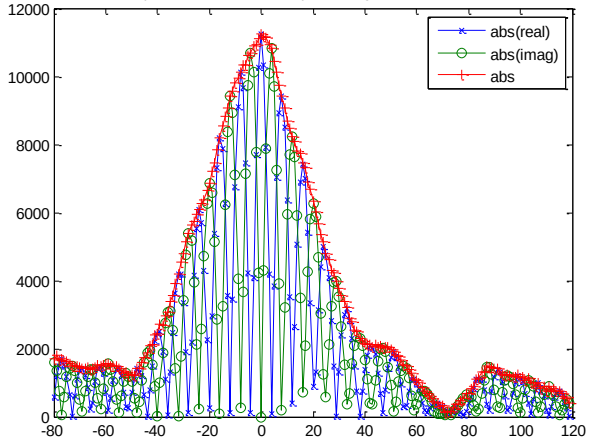

(c) VIC(2, 1)

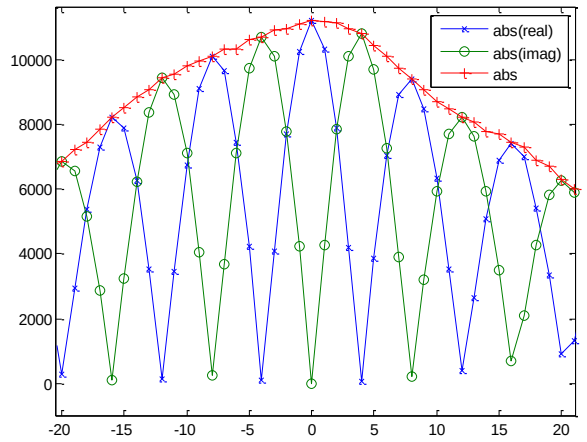

(d) Detail of VIC(2, 1)

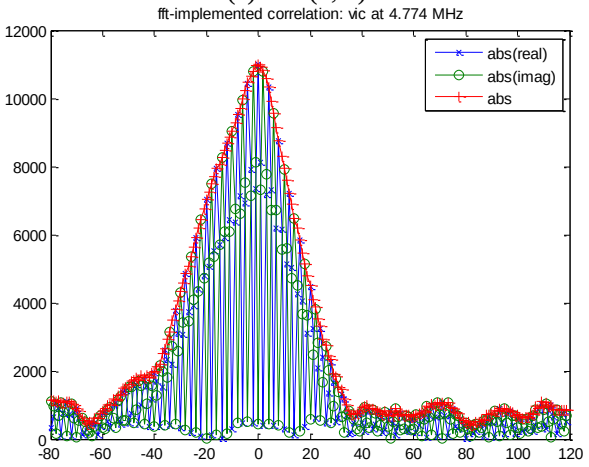

(e) VIC(4, 1)

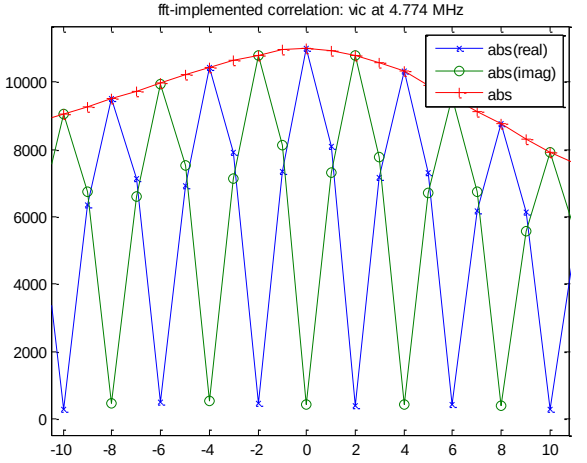

(f) Detail of VIC(4, 1)

Fig. 9 – VIC at Different IF Frequencies

In the data provided by [Borre et al., 2007], there are 8 satellites visible over the first 37 sec, which are processed into the position fixes. The top plot of Fig. 10 shows the variations over time (500 ms per data point) of the north, east, and up components of the position fixes as shown in the left plot of Fig. 11 obtained using the conventional tracking and least-square positioning methods provided by the book. In comparison, the middle and bottom plots of Fig. 10 show the variations over time of the north, east, and up components of the position fixes as shown in the middle and right plots of Fig. 11 using the VITAL method.

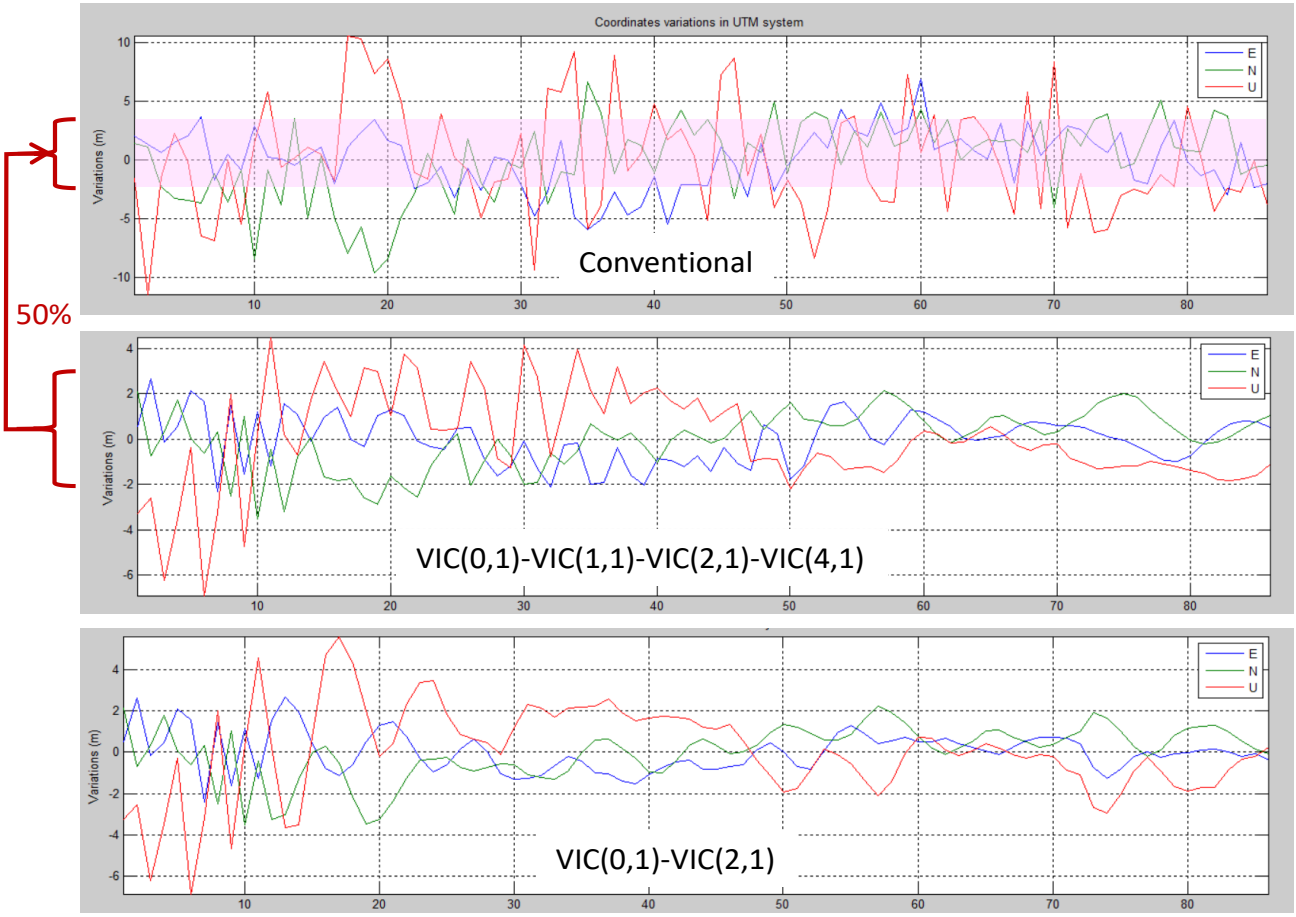

Fig. 10 – Variations in Position Fixes from Conventional & VITAL Methods (500 ms per data point)

Due to the difference in scales, the pink-shaded area (-2 m to 4 m) in the top plot of Fig. 10 represents the VITAL solution in the middle and bottom plots of Fig. 10, excluding the VIC(0, 1) in the first 10 seconds. The peak to peak errors of the VITAL solution are -2 to 2 m in the east and north components and -2 to 3 m in the up-component while those of the conventional method are -10 to 6 m in the east and north components and -10 to 10 m in the up-component, respectively. The improvement is 12 m and 15 m in peak to peak errors in the horizontal and vertical components, respectively.

The left plot of Fig. 11 shows the horizontal position errors of the conventional method. In comparison, the horizontal position errors of the VITAL method is shown in the middle and right plots of Fig. 11. Excluding the large errors when VIC(0, 1) is used at the start of processing, which is equivalent to the conventional tracking loop, the improvement is about ±5 m, consistent with what we have observed from Fig. 10.

With a simple change that uses different correlations to calculate the code phase error discriminator, we are able to improve the position errors by about 50% in both horizontal and vertical directions. Furthermore, the solution is much smoother in addition to an increase in accuracy. Additional processing results are presented in [Pany and Yang, 2017; Yang et al., 2017].

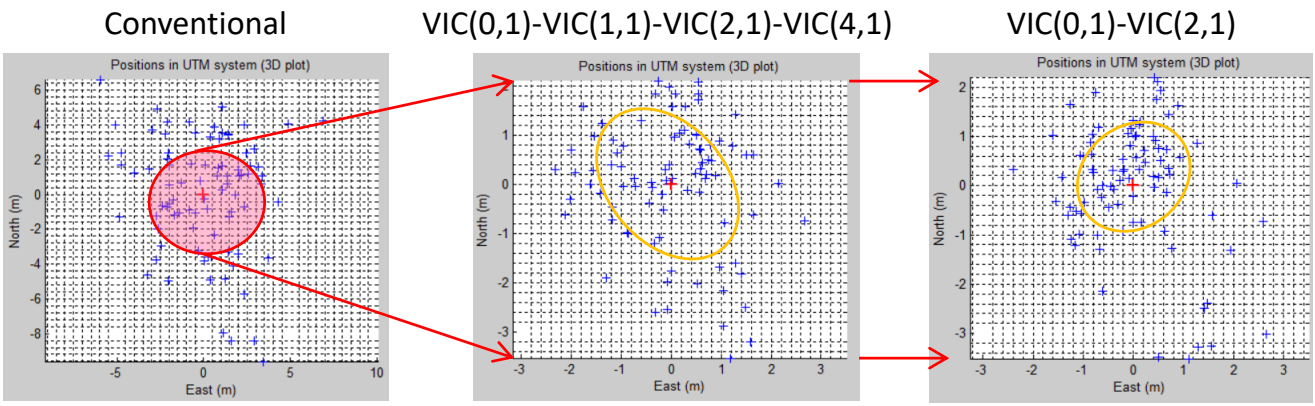

Fig. 11 – Comparison of Position Fixes from Conventional & VITAL Methods

ANALYSIS WITH SIMULATION DATA

To further analyze VITAL, a GPS signal with its parameters as close as possible to the experimental data used in the previous section was simulated with the known truth. The bit true simulated GPS C/A signal (only PRN 1) with RF at 1575.42 MHz (L1) with C/N_0 = 47 dB-Hz was down-converted to IF at 9.548 MHz and sampled with 2 bits at rate of 38.192 MHz. The simulated line-of-sight dynamics is a constant acceleration of 0.2 m/s^2 with an initial range rate is 500 m/s. Note that the simulated RF front-end filtering introduced a group delay, which appears as a bias (about 45 m) in the following range error plots.

Two 2nd-order tracking loops are used with ζ = 0.7 and B_n = 1 Hz for DLL and ζ = 0.7 and B_n = 9 Hz, respectively. The PLL uses an arctangent on the prompt correlator as its phase error discriminator for all cases. The DLL uses a normalized early-minus-late correlation power as its code error discriminator in the conventional tracking while a quadratic fitting to the three largest correlations (early, prompt, and late) as its code error discriminator for all VIC. A major difference between the conventional and VIC implementations is that the conventional tracking calculates its code errors on the correlation envelope while the VITAL on the real component of correlations after their instantaneous correction of phase tracking error based on the argument of the prompt correlator.

Figs. 12(a), (c), (e), (g), and (i) show the range errors of conventional and VIC(n, 1), n = 0, 1, 2, 4, tracking with zooming on their details in Figs. 12(b), (d), (f), (h), and (j), respectively. Note that VITAL switches at 10 s from VIC(0, 1) to VIC(n, 1) for n = 1, 2, 4. Improvement of range measurements of VIC over conventional tracking is reflected in these plots in two aspects. First, the peak-to-peak range errors are reduced more for VIC with a larger n. Second, the errors also become smoother for higher VIC. What is more interesting is the appearance of damped oscillations; with high frequency noise components suppressed more by higher VIC, the oscillation becomes smoother and slower.

The oscillation may be intuitively understood as a data compression effect of VIC. For higher VIC, the peaked correlation mainlobe has a steeper slope, which compresses more excursions of correlation into smaller errors at the output of code error discriminator. Smaller code error discriminator outputs thus steer less DLL with rate aiding from PLL (so the DLL NCO outputs are smoother) until the errors build up for a correction in one direction or the other (thus creating oscillations). Higher VIC leads to smaller variations and longer error build-ups. Since correction takes place until the error build-up reaches a similar level so the error amplitudes are about the same for different VIC as shown in Fig. 12.

Clearly VITAL allows for stable tracking of both code and carrier wherein the discriminator noise is much less for higher VIC while phase tracking is not affected by VITAL (similar to standard tracking). The noise performance of ranging is given [Van Dierendonck et al, 1992] for an infinite bandwidth signal as:

$$\sigma_\tau^2 = \frac{B_L d}{2S/N_0}\left(1 + \frac{2}{(2-d)S/N_0 T}\right)c \approx 0.7 \text{ m} \qquad (9)$$

for B_L = 1 Hz, d = 0.5 chips, T = 1 ms, $S/N_0 = 10^{(46.4\text{ dB/10})}$, and c = 293 m/chip. Since the oscillation amplitude is less than A = 1 m, the RMS of these damped sinewaves as $A/\sqrt{2}$ is close to (smaller than) 0.7 m. Code tracking errors well match the noise performance predicted from the tracking theory ([Pany and Yang, 2017]).

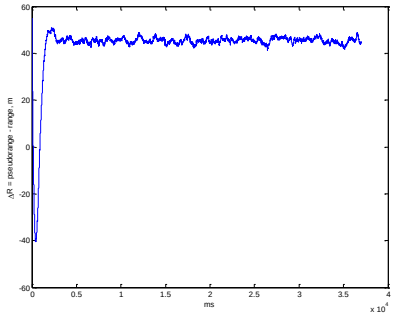

(a) Range Errors of Conventional Tracking

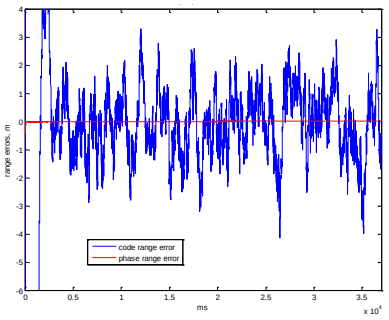

(b) Details of (a)

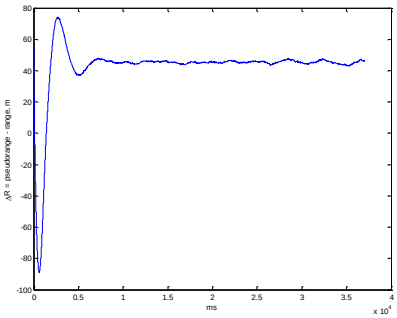

(c) Range Errors of VIC(0, 1)

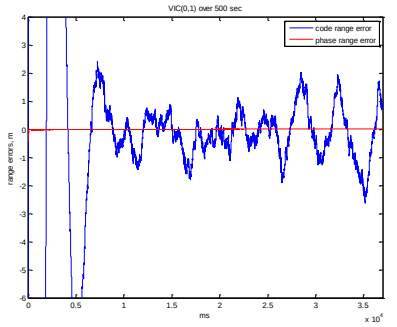

(d) Details of (c)

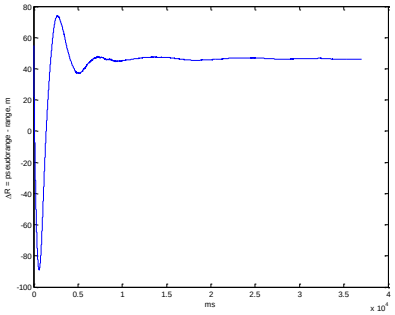

(e) Range Errors of VIC(1, 1)

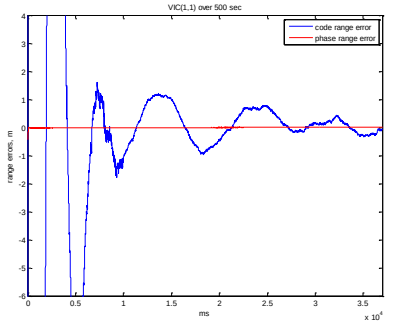

(f) Details of (e)

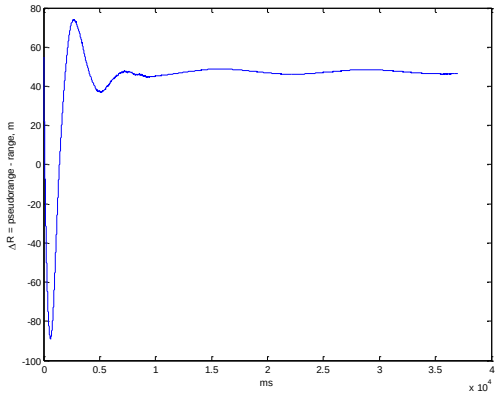

(g) Range Errors of VIC(2, 1)

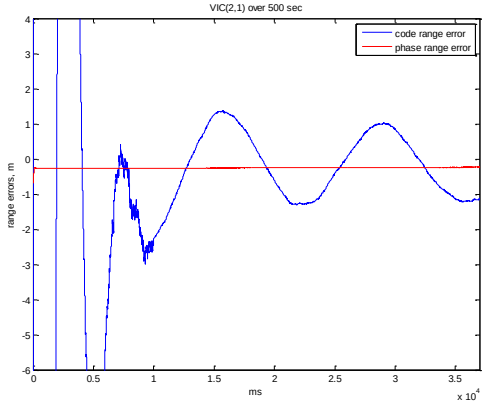

(h) Details of (g)

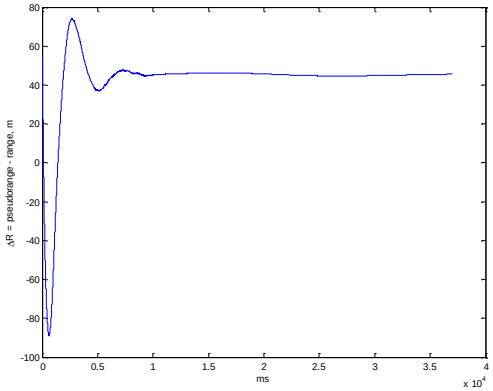

(i) Range Errors of VIC(4, 1)

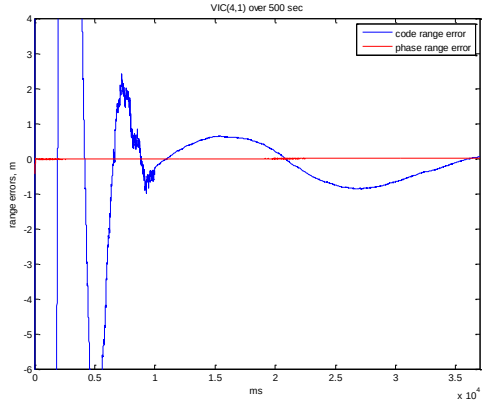

(j) Details of (i)

Fig. 12 – Comparison of Range Errors of Conventional vs. VIC(n, 1), n = 0, 1, 2, 4

One benefit of VITAL is its ability to gradually introduce carrier phase accuracy into code pseudorange. In fact, there are two well-known methods of carrier aiding of code. One carrier aiding is at the signal tracking level with rate aiding in the form of a PLL-aided DLL or an FLL-aided DLL. The other is at the measurement level with carrier phase smoothing of code pseudorange via the Hatch filter. It was suggested [Hegarty, 2016] to compare the Hatch filter with VITAL. The Hatch filter can be written as:

$$\bar{\rho}_t = \frac{1}{M}\rho_t + (1 - \frac{1}{M})(\bar{\rho}_{t-1} + \phi_t - \phi_{t-1}) \tag{10}$$

where ρ_t is the code pseudorange measurement at epoch t, ϕ_t is the carrier phase measurement at epoch t, $\bar{\rho}_t$ is the carrier smoothed code at epoch t, and M is the length of the Hatch filter.

Consider the same simulation example as above. Fig. 13(a) shows the code pseudorange measurements from a conventional DLL loop. Fig. 13(b) shows the carrier phase measurements from a conventional PLL loop. Fig. 13(c) shows the code pseudorange measurements in Fig. 13(a) smoothed by the carrier phase measurements in Fig. 13(b) for three filter lengths of M = 10 (blue), 100 (green), 1000 (red) samples, respectively, with a sampling rate of 1 kHz (1 ms). Note that the chosen filter length of M = 10, 100, and 1000 correspond to a smoothing time interval of 0.01 s, 0.1 s, and 1 s, respectively, due to the short duration of the simulated data set. In practice, however, a longer smoothing time interval of either 10 s or 100 s is usually used. Fig. 13(d) shows the code pseudorange measurements from a tracking loop that switches from the conventional early-minus late code error discriminator to VIC(2, 1) at 10 s.

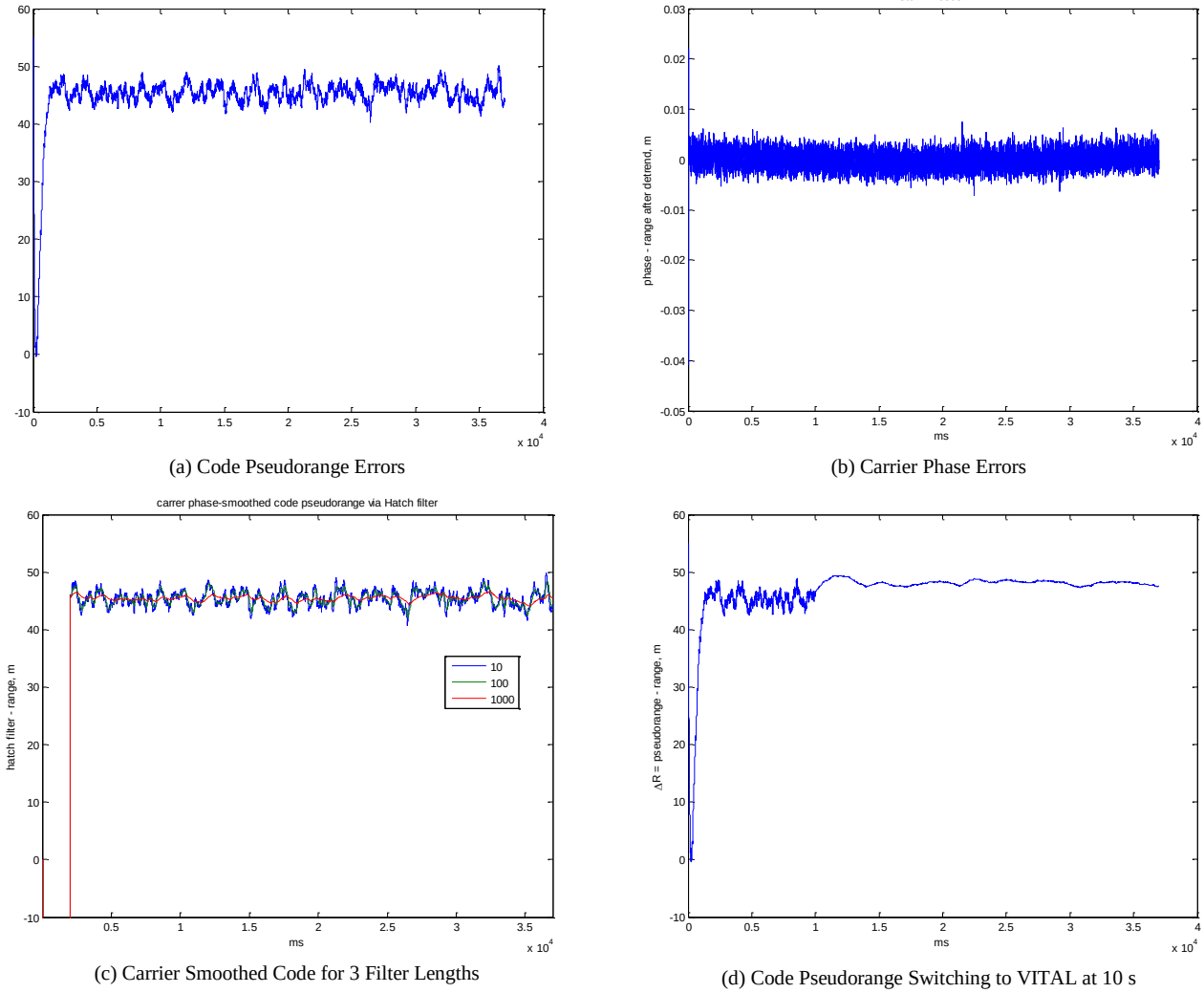

(a) Code Pseudorange Errors

(b) Carrier Phase Errors

(c) Carrier Smoothed Code for 3 Filter Lengths

(d) Code Pseudorange Switching to VITAL at 10 s

Fig. 13 – Comparison of VITAL and Hatch Filter Outputs

It is clear from Fig. 13 that the Hatch filter with a length of 1000 samples (1 s) is comparable to VIC(2, 1) in terms of smoothness. However, it is well known that carrier-smoothed code measurements can suffer from a bias in an ionospheric storm due to code and carrier divergence and its lasting effect due to the long memory of the smoothing filter. Advanced techniques such as adaptive [Kim et al., 2007] and nonlinear [Sen and Rife, 2008] are developed to deal with the errors. In contrast, the sharpness of the main peak of VIC is not affected much by the code and carrier divergence and so is not the VITAL operations.

CONCLUSIONS

In this paper, we provided the details of an implementation of the variable IF tracking loop (VITAL) and demonstrated its performance in terms of increased code tracking and positioning accuracy with simulated data and real-world GPS C/A-code signals.

VITAL is based on the idea of variable IF correlation (VIC) first introduced in [Yang, 2015; 2016] and then extended from BPSK signals to OFDM subcarriers [Yang and Soloviev, 2017]. The combined code and carrier correlation can satisfy the conflicting requirements of a wide correlation peak for fast acquisition and a sharp narrow peak for accurate tracking and mitigation of multipath and spoofing signals. Furthermore, the method may enable many narrowband communications signals, which have been precluded in the past from being considered for precise timing due to lack of bandwidth, as radio signals of opportunity now for ranging and positioning.

As recently analyzed in [Pany and Yang, 2017], by spectrally shifting GPS signals, VITAL provides a real increase in code tracking accuracy. However, the improvement comes at a price, that is, the code and carrier estimates become correlated. On the one hand, the VITAL concept offers a gradual way to extend the carrier accuracy into the code tracking. On the other hand, any carrier tracking error, which is more likely (and easily) to occur, can spill over into the code tracking error. Work is under way to characterize such correlation toward a balanced design of VITAL that can fall back from VIC(i, 1) to VIC(0, 1) as needed while benefiting from a sustained performance improvement from carrier phase.

REFERENCES

[1] J. Betz, "The Offset Carrier Modulation for GPS Modernization," *Proc. of the ION 1999 NTM*, San Diego, CA, Jan. 1999.

[2] D. Borio, "Double Phase Estimator: a New Unambiguous BOC Tracking Algorithm," *IET Radar, Sonar and Navigation*, 8(7), 729-741, 2014.

[3] K. Borre, D.M. Akos, N. Bertelsen, P. Rinder, S.H. Jensen, *A Software-Defined GPS and Galileo Receiver: A Single-Frequency Approach*, Birkhäuser Basel, 2007.

[4] P. Bidigare, U. Madhow, R. Mudumbat, and D. Scherber, "Attaining Fundamental Bounds on Timing Synchronization." *Proc. of ICA*SSP, 2012.

[5] L. Chen, O. Julien, P. Thevenon, D. Serrant, A.G. Pena, and H. Kuusniemi, "TOA Estimation for Positioning with DVB-T Signals in Outdoor Static Tests," *IEEE Trans. on Broadcasting*, Vol. 61, No. 4, Dec. 2015, pp 625-638.

[6] J.A. del Peral-Rosado, *Evaluation of the LTE Positioning Capabilities in Realistic Navigation Channels*, Universitat Autonoma de Barcelona Ph.D Dissertation, 2014. [6] P. Fine and W. Wilson, "Tracking Algorithm for GPS Offset Carrier Signals," *Proc. of ION NTM*, January 1999.

[7] C. Hegarty, Private Conversation, Nov. 2016.

[8] M.S. Hodgart, P.D. Blint, and M. Unwin, "Double Estimator: A New Receiver Principle for Tracking BOC Signals," *InsideGNSS*, Spring 2008.

[9] O. Julien, C. Macabiau, M.E. Cannon, and G. Lachapelle, "ASPeCT: Unambiguous Sine-BOC(n,n) Acquisition/Tracking Technique for Navigation Applications," *IEEE Trans. on Aerospace and Electronics Systems*, Vol. 43, No. 1, January 2007.

[10] E.D. Kaplan and C.J. Hegarty (Eds.), *Understanding GPS: Principles and Applications* (2nd Ed.) Artech House Publishers, Norwood, MA, 2006.

[11] E. Kim, T. Walter, and J.D. Powell, "Adaptive Carrier Smoothing Using Code and Carrier Divergence," ION-NTM 2007, Jan. 2007, San Diego, CA.

[12] J.A. Namzer, M.D. Sharp, and D.R. Brown, III, "Bandpass Signal Design for Passive Time Delay Estimation," *Proc. of 50th Asilomar Conference on Signals, Systems and Computers,* Pacific Grove, CA, Nov. 2016.

[13] C. O'Driscoll, J.A. Avila Rodriguez, and R. Ioannides, "Bandlimiting and Dispersive Effects on High Order BOC Signals," *Proc. of ION GNSS+*, Portland, OR, Sept. 2016.

[14] C. Palestini, *Synchronization and Detection Techniques for Navigation and Communication Systems*, Ph.D. Dissertation, University of Bologna, March 2010.

[15] T. Pany, *Navigation Signal Processing for GNSS Software Receivers*, Artech House Publishers, Norwood, MA, 2010.
[16] T. Pany and C. Yang, "Code and Carrier Tracking for Spectrally Asymmetric Signals," *ION-ITM*, Monterey CA, January 2017.
[17] M. Paonni, J.T. Curran, M. Bavaro, and J. Fortuny-Guasch, "GNSS Meta-Signals: Coherent Composite Processing of Multiple GNSS Signals," *ION-GNSS+ 2014*, Sept. 2014.
[18] S. Sen and J. Rife, "Reduction of Ionosphere Divergence Error in GPS Code Measurement Smoothing by Use of a Non-Linear Process," *Proc. of IEEE/ION PLANS*, May 2008, Monterey, CA, 312-320.
[19] D. Serant, O. Julien, L. Ries, P. Thevenon, and M. Dervin, "The Digital TV Case – Positioning with Signals of Opportunity Based on OFDM Modulation," *InsideGNSS*, Nov/Dec 2011, 54-62.
[20] K. Shamaei, J. Khaife, and Z.M. Kassas, "Performance Characterization of Positioning in MISO LTE Systems," *Proc. of ION GNSS+*, Portland, OR, Sept. 2016.
[21] P. Thevenon, S. Damien, O. Julien, C. Macabiau, M. Bousquet, L. Ries, Lionel, and S. Corazza, "Positioning Using Mobile TV Based on the DVB-SH Standard," *Navigation: J. of the Institute of Navigation*, Vol. 58, No. 2, Summer 2011, 71-90.
[22] A.J. Van Dierendonck, P. Fenton, and T. Ford, "Theory and Performance of Narrow Correlator Spacing in a GPS Receiver," *Navigation: J. of the Institute of Navigation*, Vol. 39, No. 3, Fall 1992.
[23] C. Yang, "Joint Code and Carrier Correlation for GNSS Signals with Peak Sharpening," *ION GNSS+2015*, September 2015.
[24] C. Yang, "Sharpen the Correlation Peak: A Novel GNSS Receiver Architecture with Variable IF Correlation," *Navigation: Journal of the Institute of Navigation*, 63(3), Fall 2016, 249-265.
[25] C. Yang, L. Chen, O. Julien, R.Z. Chen, and A. Soloviev, "Carrier Phase Tracking of OFDM-Based DVB-T Signals for Precision Ranging," *ION-GNSS+ 2017*, Portland, OR, September 2017.
[26] C. Yang, T. Pany, and A. Soloviev, "An Implementation of Variable IF Tracking Loop (VITAL) and Initial Test Results," To Appear in *Navigation: J. of the Institute of Navigation*, Accepted for Publication on Aug. 14, 2017.